Alternative steel lattice structures for wind energy converters

Jovasevic, Slobodanka; Correia, José; Pavlovic, Marko; Dantas, Rita; Rebelo, Carlos; Veljkovic, Milan; de Jesus, Abilio M.P.

DOI
10.1108/IJSI-05-2019-0042

Publication date
2019

Document Version
Final published version

Published in
International Journal of Structural Integrity

Received 1 May 2019
Revised 9 August 2019
Accepted 10 August 2019

Alternative steel lattice structures for wind energy converters

Slobodanka Jovasevic
Faculty of Science and Technology, University of Coimbra, Coimbra, Portugal
José Correia
Department of Civil Engineering, Faculty of Engineering, University of Porto, Porto, Portugal
Marko Pavlovic
Delft University of Technology, Delft, The Netherlands
Rita Dantas
Department of Mechanical Engineering, University of Porto, Porto, Portugal
Carlos Rebelo
Faculty of Science and Technology, University of Coimbra, Coimbra, Portugal
Milan Veljkovic
Delft University of Technology, Delft, The Netherlands, and
Abilio M.P. de Jesus
Department of Mechanical Engineering, University of Porto, Porto, Portugal

Abstract

Purpose – In the last decades, the demand and use of renewable energies have been increasing. The increase in renewable energies, particularly wind energy, leads to the development and innovation of powerful wind energy converters as well as increased production requirements. Hence, a higher supporting structure is required to achieve higher wind speed with less turbulence. To date, the onshore wind towers with tubular connections are the most used. The maximum diameter of this type of tower is limited by transportation logistics. The purpose of this paper is to propose an alternative wind turbine lattice structure based on half-pipe steel connections.

Design/methodology/approach – In this study, a new concept of steel hybrid tower has been proposed. The focus of this work is the development of a lattice structure. Therefore, the geometry of the lattice part of the tower is assessed to decrease the number of joints and bolts. The sections used in the lattice structure are constructed in a polygonal shape. The elements are obtained by cold forming and bolted along the length. The members are connected by gusset plates and preloaded bolts. A numerical investigation of joints is carried out using the finite element (FE) software ABAQUS.

Findings – Based on the proposed study, the six "legs" solution with *K* braces under 45° angle and height/spread ratio of 4/1 and 5/1 provides the most suitable balance between the weight of the supporting structure, number of bolts in joints and reaction forces in the foundations, when compared with four "legs" solution.

Originality/value – In this investigation, the failure modes of elements and joints of an alternative wind turbine lattice structures, as well as the rotation stiffness of the joints, are determined. The FE results show good agreement with the analytical calculation proposed by EC3-1-8 standard.

Keywords Built-up polygonal sections, Preloaded gusset-plate connections, Steel hybrid towers, Tower geometry

Paper type Research paper

International Journal of Structural Integrity
Vol. 12 No. 1, 2021
pp. 48-69

1757-9864
DOI 10.1108/IJSI-05-2019-0042

The authors acknowledge the support of the European Commission's Framework Programmes "Horizon 2020" programme through the Marie Skłodowska-Curie Innovative Training Networks (ITN) "AEOLUS4FUTURE – Efficient Harvesting of the Wind Energy" (H2020-MSCA-ITN-2014: Grant Agreement No. 643167) and RFCS – Research Fund for Coal and Steel programme through the Grant Agreement RFSR-CT-2015-00021-SHOWTIME.

1. Introduction

Nowadays, global warming is one of the main concerns of our society and, as such, there is an increasing need to change the behaviours that are causing it. The principal activities responsible for the emission of greenhouse gases are energy production and industry. In 2014, the energy obtained from fossil fuels represented 81 per cent of world energy production (Letcher, 2017).

However, in 2014, the European Union aimed to have at least 27 per cent of the total energy consumption covered from the renewable energy sources (EWEA, 2017). Onshore wind energy as a renewable energy source represents a very competitive alternative to fossil fuels. By the end of 2015, the installed capacity of renewable wind energy was more than 141 GW in Europe (EWEA, 2015). The construction of more powerful wind energy converters (WEC) is required due to the increasing demand for renewable energies. The power produced by a wind turbine highly depends on the wind velocity. In this way, higher wind turbine towers are fundamental to reach zones with the less turbulent and faster wind, thus obtaining more power (Figure 1) (Letcher, 2017; Heistermann, 2011).

Up to 30 per cent of the total WEC cost is due to tower construction. The tower height increase leads to more difficult and more expensive transportation, assembly, erection and maintenance (Hau, 2006). However, as stated before, with the height increase, the generated energy increases as well.

In this way, several scientific and technical events have been organized with the purpose of generating scientific knowledge related to wind energy technology. In 2017, Winercost event (International Conference on Wind Energy Harvesting) brought together the present expertise on the built-environment wind energy technology in order to investigate smart cities methodologies and discussed a variety of topics, such as wind characteristics and loads; structures, materials and dynamics; grid integration, operations and control; markets, strategies, policies and socio-economics smart cities; and environmental aspects (Rebelo *et al.*, 2018).

Nowadays, the most frequently used tower types for WEC are steel, concrete or hybrid tubular towers. One of the tallest steel tubular towers installed is Vestas 3 MW wind turbine with 166 m hub height (Figure 2(a)). The diameter of this WEC tower model reaches 6.5 m in

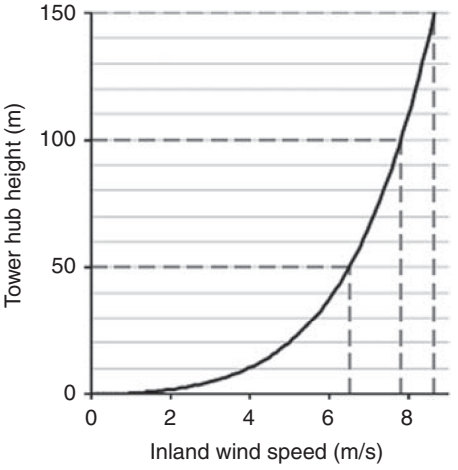

Source: Heistermann (2011

Figure 1.
Inland wind speed increasing with hub height

the base, which implies that base segments are made of several pieces to satisfy public road transport limitations. However, this has resulted in transportation and installation cost increase (Vestas Wind Systems A/S, 2016).

In the beginning, the design and optimization of lattice structures by using tubular joint were studied in the offshore field, because these platforms are formed by a jacket structure (Duthoit and Falzarano, 2018). Gong (Gong, 2011) suggested a design and an analysis of two different types of transition piece models under different load conditions applied to wind turbine support structures. A design concept for wind turbine towers, which aims to replace the traditional support structures by simple lattice support structures, was proposed by Muskulus (2012). Moreover, Muskulus and Schafhirt (2014) presented a review on the design optimization of wind turbine support structures, where the challenges and possible approaches for structural optimization are highlighted as well as design recommendations are suggested.

Therefore, many works have been developed to replace traditional onshore wind turbine towers by hybrid structures (tubular + lattice tower). As previously mentioned, this modification allows higher towers, and consequently, more wind energy can be produced. Thus, there are many topics related to structural design, such as static and dynamic behaviour, fatigue analysis, wind loads, stability, structural integrity, efficiency, economic variables and security, that have been studied (Américo *et al.*, 2014; Alvarez-Anton *et al.*, 2016; Seidel *et al.*, 2016; Wang *et al.*, 2016).

Recently, a few other concepts have been developed. Ruukki (2011) used a lattice structure for 2.5 MW turbine to reach 160 m height (Figure 2(b)). For heights beyond 130 m, General Electric – Renewable Energy (2014) proposed a new enclosed lattice space frame assembled on-site (Figure 2(c)). This new solution makes the tower cost-effective and utilizes standard logistic (General Electric – Renewable Energy, 2014). Moreover, Suzlon Energy Limited (2016) designed a 120 m hybrid wind turbine tower with 2.1 MW rated power and a four-legged lattice structure with "L" shaped cross-sections. The instability of compressed members is overcome using intermediate struts (Figure 2(d)). Besides, Ruukki proposed a new type of open six-corner polygonal sections to improve the stability of members in lattice towers.

The lattice tower structure is an interesting solution to overcome transportation restrictions of public roads and achieve lighter structures (Gencturk *et al.*, 2012; Mohammadi *et al.*, 2018). Besides, these structures are characterized by large-based areas capable of better

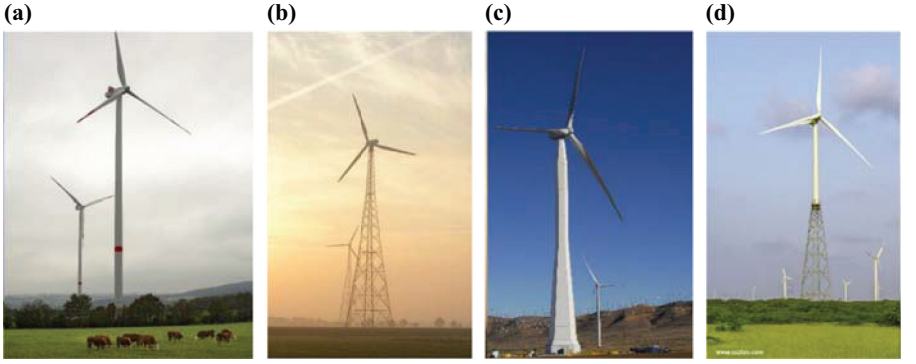

Figure 2.
Types of wind turbine towers

Notes: (a) RUUKKI lattice tower; (b) GE space frame lattice tower; (c) Suzlon hybrid tower; (d) Vestas LDST tubular tower

withstanding lateral loads applied and by a design that reduces wind loads (Gencturk *et al.*, 2014). However, the assembly task, as well as the maintenance of bolted connections, is more arduous and difficult. Fatigue loads are also a relevant issue to be aware of lattice towers (Gencturk *et al.*, 2012). Recently, Nunez-Casado *et al.* (2017) developed assembly strategies of wind turbine towers with the aim to minimize the fatigue damage. Other studies on the fatigue design of transition piece for onshore hybrid wind turbines, considering the multi-axial fatigue damage criterion, have been proposed (Farhan *et al.*, 2018).

Therefore, a hybrid tower design approach is being developed within the SHOWTIME (2014) project (Steel Hybrid Onshore Wind Towers Installed with Minimal Effort), where the lattice structure is used as the lower part of the tower and the tubular tower structure as the upper part. These two parts are connected by a transition piece. With this approach, the base diameter is reduced, hence facilitating the tower transportation. Additionally, optimized technology for steel tubular towers is being used for the upper portion of the tower, whereas the expression in the height is being achieved with lattice structure (Hau, 2006; Figueiredo and Carlos, 2013). Another advantage is that high cranes for tower installation can be avoided by using a lattice structure for a tubular tower and turbine installation. Several types of support structures for wind energy towers, particularly structures with tubular elements, have been proposed. One of the main goals of this research project is to use the new types of bolted polygonal cross-sections introduced by Ruukki (2011). In this type of structure, members are composed of built-up open cross-sections connected with preloaded bolts (Figure 3).

These section segments are manufactured by cold forming, so that the members are very thin and have a quite large diameter in comparison with their thickness. Therefore, resistance to global member buckling is increased. Local buckling can, however, be expected before section yielding due to the slenderness of cold-formed member. For this particular case, coupon tests on individual cold-formed section parts were performed by (Garzon, 2013). The results have shown that, due to cold forming, the yield strength for the section bent with 110° increases by about 29 per cent compared to the virgin plates.

Several studies were made to establish a comparison of polygonal and circular cross-sections for different slenderness ratios of D/t. Very thin-walled slender tubes with a ratio of the flat width and thickness b/t between 63 and 630 were tested by Bulson (1969). His results for tubes up to 18 sides showed a linear relationship between maximum strength and the number of sides. The polygonal sections with more than 22 sides collapse in the same mode as the circular tube. Therefore, after 22 sides, the polygonal tube did not have any structural

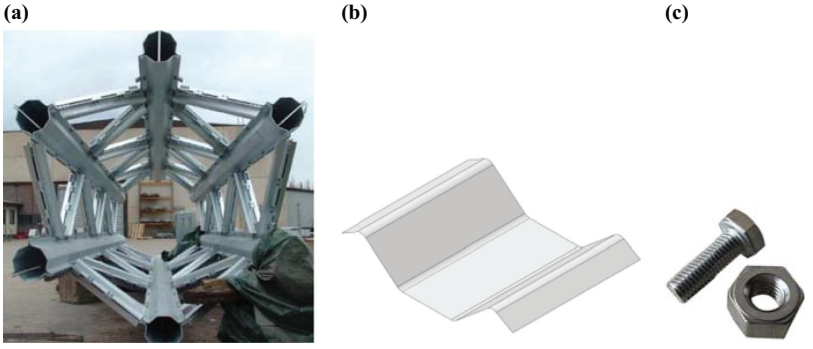

Notes: (a) Lattice tower with built-up polygonal sections; (b) polygonal section segment; (c) preloaded bolts details

Figure 3.
Lattice structure for a tubular tower and turbine instalation

advantage. Garzon's (2013) study showed a good agreement with Bulson's results for polygonal cross-sections with a *b/t* ratio between 69 and 191, but not for the polygonal tube with *b/t* ratio between 18 and 39. For these ratios (18 and 39), the maximal strength capacity under compression is reached for polygonal tubes with 16 sides. A small difference is observed in the resistance for the tubes with 12 sides. After 16 sides, the polygonal tube had no longer structural advantage over the circular tube. Therefore, polygonal sections with a number of sides lower than 12 were chosen for the members of the lattice structure.

One of the important parameters in global structural behaviour is the behaviour of joints in a structure. Currently, codes use the effective length method to assess the stability of structures (Webber *et al.*, 2015). The effective length of compressed members (both pylon and brace members) is calculated considering non-linear moment–rotation characteristics of joints. An extensive study has been carried out due to the lack of this information in the current design codes (Webber *et al.*, 2015).

The main objective of this work is the optimization and detailed design of connections between polygonal members built on-site using preloaded bolts. The geometry of the lattice structure part and cross-sections of the members were determined from the parametric study. An optimization study for 120 m lattice structure models was made considering the number of "legs" and lattice structure height/spread (*H/S*) ratio, where the weight and the number of joints were discussed and taken into account in the analysis. Furthermore, finite element (FE) models of connections between polygonal built-up members were developed to determine resistance and moment–rotation characteristics. The numerical simulation of the half-pipe steel connections, consisting of a pylon and a secondary bracing, was based on two steps to simulate the bolt preload (the first step – using thermal contraction) and actuator loading (the second step – using displacement in vertical direction applied to the secondary bracing). In this study, two types of half-pipes steel connections were studied – the vertical element called pylon and the secondary element with horizontal or 45° angle bracing. These analyses were conducted considering two types of joints, bolted and welded joints, between the pylon and gusset plate linking to bracing. A quasi-static analysis was used.

2. Lattice geometry

A batch of different lattice structure geometries is designed for ultimate limit state. An iterative design approach is used. The ASHES aeroelastic and SAP2000 structural analysis software are used (Jovašević *et al.*, 2017). The parameters used in this study are targeting the ratio between the height of the tubular and lattice structure, the *H/S* ratio of lattice structure and the number of joints/bolts in the structure. The following parameters are defined for case studies:

- wind turbine power: 5 MW;
- tubular segment height: 100 m;
- lattice structure height: 120 m;
- number of "legs": four and six; and
- lattice structure *H/S* ratio =1/1; 2/1; 3/1; 4/1; 5/1; 6/1.

The most advantageous geometry of the lattice structure face was determined to compare four different solutions (Figure 4). For each proposed solution, the brace angle was varied with the 5° increment between 30° and 50° for four "legs" towers and 35° and 55° for six "legs" towers.

In this analysis, the used optimization criterion evaluated in terms of mass and number of joints. The evaluation of four "legs" lattice structures in terms of mass and number of joints of

the lattice structure is represented in Figure 5(a). In the plot of this figure, it can be observed that the optimal solution is achieved for the second bracing layout with a brace angle of 45°; therefore, this solution will be used for further study. In the same way, six "legs" structures were compared in Figure 5(b). Also, two solutions were assessed: one chosen from four "legs" lattice structure study and another one with *K* bracing layout (Figure 4). As an optimal solution, *K*-braced structure was selected. Furthermore, for both structures, with four and six "legs", further parametric study was performed for a 45° brace angle.

For the next stage of the analysis, a 3D model of the lattice structure was created by varying braces' cross-section along the height, while the columns' cross-section was considered constant. The braces angles are equal to 0° and 45°, respectively, for the welded and bolted joints under consideration. The weight and the number of joints of 120 m lattice models were compared for different *H/S* ratios of four "legs" and six "legs" lattice structures in Figure 6.

The comparison between suggested solutions is based on the following parameters:

- lattice structure weight;
- number of joints in the structure;
- estimated number of bolts (for N_{Ed} in brace elements); and
- foundation reaction force.

The results of the parametric study for four "legs" and six "legs" structures are demonstrated in Figure 6. The comparison is represented as a dependency of the structure mass and the number of joints (estimated number of the bolts). At this stage, presented in Figure 6(a), the only mass of lattice portion of the tower was accounted for. Four "legs" and six "legs" structures with the lowest mass were checked for *H/S* ratios of 5/1 and 3/1. Hence, these three solutions were used for further study related with the estimated number of bolts (Figure 6(b)). In the further study, the entire tower was analyzed (including a tubular portion of the tower). The number of bolts was calculated for each solution according to EC 3 Part 1-8. The design of

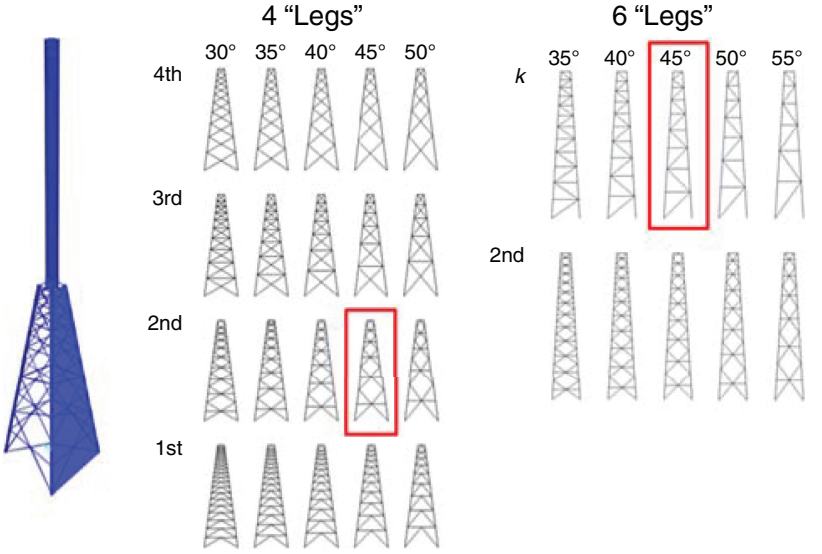

Figure 4.
Parametric study – brace geometry

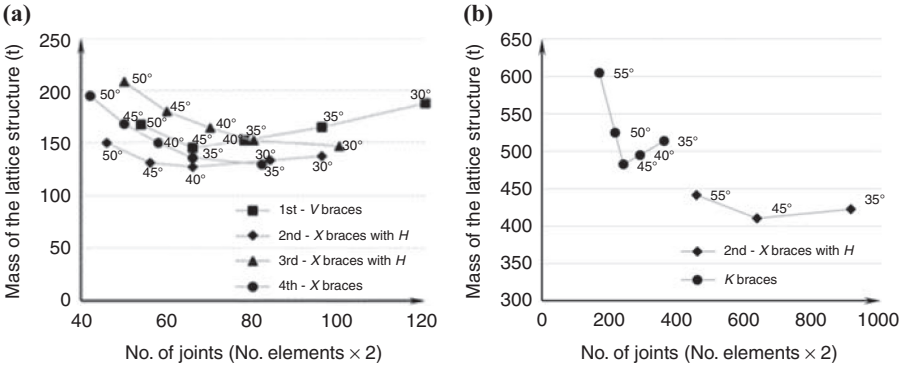

Figure 5.
Comparison of 2D models

Notes: (a) Four-legged lattice structures; (b) six-legged lattice structures. structures are shown in Figure 4

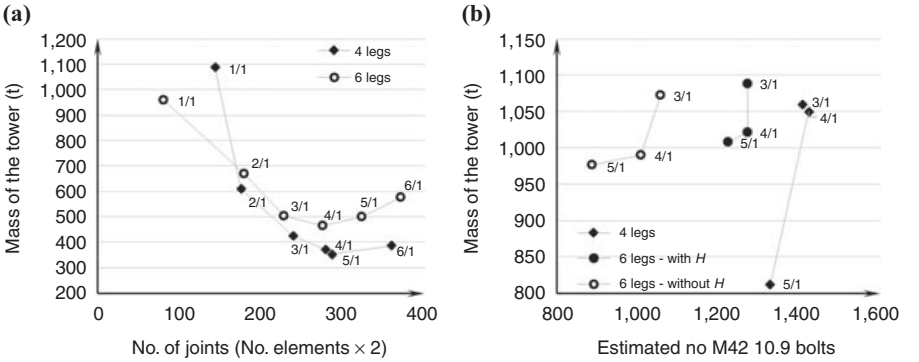

Figure 6.
The selected geometries for mass and (a) number of connections; (b) estimated number of bolts

connections has shown that six "legs" lattice structure with *K* braces (without horizontals) requires the lowest number of bolts.

The height overspread (*H/S*) ratios of 3/1, 4/1 and 5/1 show more promising results; therefore, further analysis is performed on 120 m lattice with the mentioned *H/S* ratio.

The six "legs" lattice structure without horizontal braces (called *H* in Figures 5–7) was investigated. The four "legs" design optimization without horizontal bracing was not considered, as the elimination of any horizontal bracing causes an out of plane deformation at *X*-braces cross-points. To compare the six-legged structures with and without horizontals and the four-legged lattice structure, the same set of results were obtained and compared for all the designed structures. Moreover, the mass and estimated number of bolts for four- and six-legged structures with and without horizontal bracing are compared in Figure 6(b). For these cases, the cost of material for lattice structure manufacturing was compared (Figure 7).

Furthermore, it can be seen in Table I that with the increase of the *H/S* ratio, the maximum tensile force in the foundation increases as well. This occurs due to the smaller lever arm at the ground level to resist the overturning moment. So, the structures with higher *H/S* ratios need heavier foundations to overcome the overturning phenomena. Besides, as expected, the tensile force at the ground for six "legs" lattice structure with *H/S* ratio of 4/1 and 5/1 is smaller than for the similar ratio in four "legs" lattice structure.

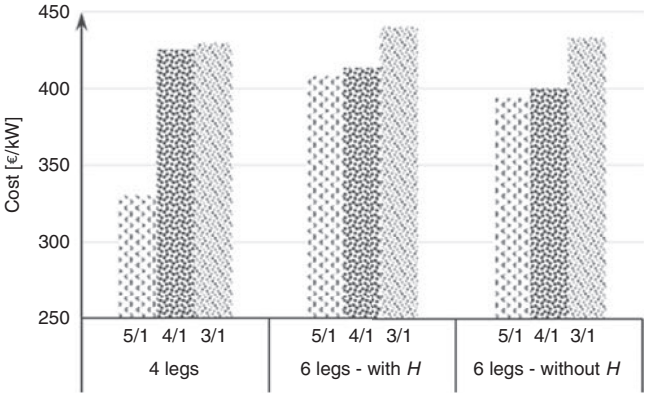

Figure 7.
Cost of material for lattice structure manufacturing

H/S	R_3 (kN)
4 legs	
3/1	9,281
4/1	15,423
5/1	22,847
6 legs without H	
3/1	10,514
4/1	14,403
5/1	20,572

Table I.
Maximal tensile force in the foundation

The four-legged tower with *H/S* ratio equal to 5/1 is the most economical solution when it comes to the weight of the steel structure being 16 per cent lighter than the 6-legged tower with the same *H/S* ratio. However, the reaction forces on foundations are higher, approximately 10 per cent. Regarding the estimated number of bolts, six-legged tower has 33 per cent fewer bolts compared to four-legged tower. Taking into account the fact that an increase in installed number of bolts increases the labour cost, the solution chosen to be more optimal is six-legged tower. Both *H/S* ratios, 4/1 and 5/1, should be investigated more in detail, taking into account labour and foundation costs.

3. Connection configuration

The joints analyzed in this work are depicted in Figure 8(a). The brace is the second member of the joint (horizontal or with 45° angle in Figure 8(b) and (c), respectively), and the pylon is the main member (vertical in Figure 8 (right)). Gusset-plate connections with preloaded bolts are used with the aim of maintaining the simplicity of the joint bolted *in situ*.

In this study, four case study joints were analyzed: B90, B45, W90 and W45. In these denominations, "B" and "W" represent bolted and welded pylon cross-section types (Figure 9), whereas "90" and "45" are the angles between pylon and brace element.

3.1 Cross-section type

Brace and pylon members of the lattice structure are composed by connecting cold-formed thin-walled open sections along the length with preloaded bolts in order to create a closed

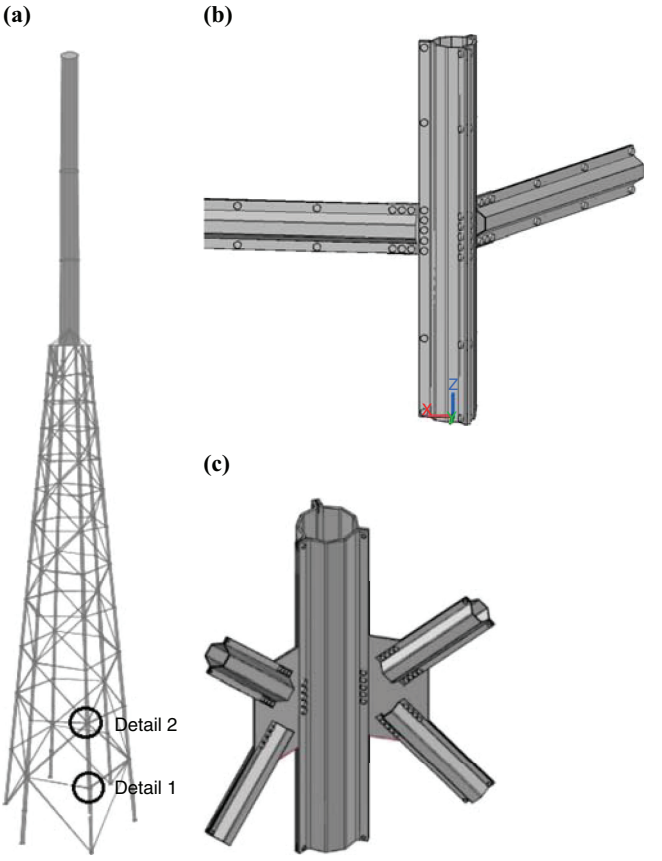

Figure 8.
Joint between pylon and brace members

Notes: (a) Global structural model; (b) joint Detail 1; (c) joint Detail 2

polygonal cross-section. The pylon is composed of three pieces bolted together along the length and forming a nine-sided polygonal cross-section. The brace is built out of two pieces bolted together along the length forming a hexagonal cross-section (Figure 9) (Jovašević *et al.*, 2017). Polygonal built-up sections are used instead of circular hollow sections due to higher ultimate strength. Additionally, polygonal members and connections between these members have a longer fatigue life as a result of the fatigue behaviour of preloaded high-strength bolted joints, which can bear higher fatigue loads than welded joints under shear or friction loads (Ozturk *et al.*, 2016; Jaspart and Weynand, 2016).

3.2 Dimensions

The characteristics of the joint (which is composed of the brace, the column and the gusset plate) are organized into two groups: dimensions (Table II) and mechanical properties (Table III):

(1) Dimensions:

- Column: column diameter (D_c), column thickness (t_c) and column bending radius (r_c).

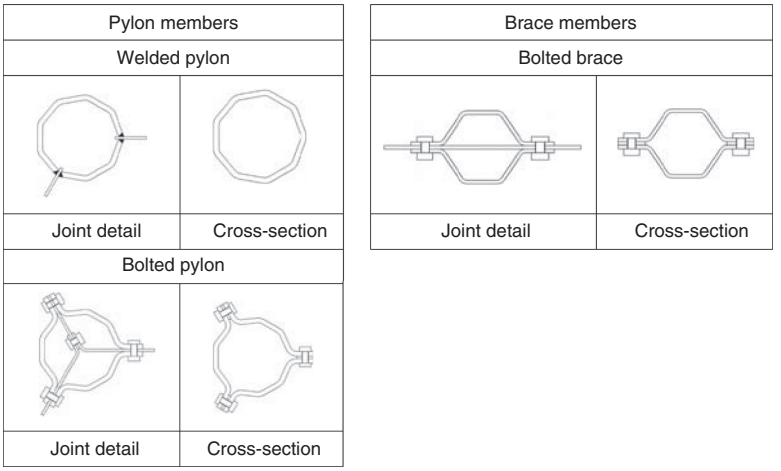

Figure 9.
Cross-sections geometry and joint details

B90		B45		W90		W45		M20		M12	
D_c	325	D_c	325	D_c	325	D_c	325	d_0	22	d_0	13
t_c	12	t_c	12	t_c	20	t_c	12	d_b	20	d_b	12
D_b	200	D_b	200	D_b	200	D_b	200	d_{nb}	25.4	d_{nb}	25.4
t_b	5	t_b	10	t_b	5	t_b	5	t_{nb}	13	t_{nb}	8
h_{gp}	380	h_{gp}	960	h_{gp}	380	h_{gp}	960	d_{hb}	25.4	d_{hb}	25.4
t_{gp}	6	t_{gp}	8	t_{gp}	15	t_{gp}	10	t_{hb}	10	t_{hb}	16
r_c	12	r_c	12	r_c	20	r_c	12	A_s	245	A_s	84.3
r_b	5	r_b	10	r_b	5	r_b	5				
r_{gp}	6	r_{gp}	8	r_{gp}	15	r_{gp}	10				
Bolts	M20	Bolts	M20	Bolts	M20	Bolts	M12				
$p_{2,cb}$	60	$p_{2,cb}$	110	$p_{1,bb}$	70	$p_{1,bb}$	35				
$p_{1,bb}$	70	$p_{1,bb}$	70	$e_{1,bb}$	35	$e_{1,bb}$	20				
$e_{1,bb}$	35	$e_{1,bb}$	35	$e_{2,bb}$	30	$e_{2,bb}$	20				
$e_{2,bb}$	30	$e_{2,bb}$	30								
$e_{1,cb}$	40	$e_{1,cb}$	40								
$e_{2,cb}$	40	$e_{2,cb}$	40								

Table II.
Connections and bolts dimensions (mm)

Member		Bolt	
f_y	355	$f_{y,b}$	900
f_u	510	$f_{u,b}$	1,000

Table III.
Mechanical properties (MPa)

- Brace: brace diameter (D_b), brace thickness (t_b) and brace bending radius (r_b).
- Gusset plate: gusset plate height (h_{gp}), gusset plate thickness (t_{gp}) and gusset plate bending radius (r_{gp}).
- Bolts: distance between rows on column ($p_{x,cb}$), distance between bolt rows on brace ($p_{x,bb}$), edge distance ($e_{x,cb}$, $e_{x,bb}$), bolt head diameter (d_{hb}), bolt head thickness (t_{hb}), bolt hole clearance (d_0), nominal bolt diameter (d_b), nut diameter (d_{nb}), nut thickness (t_{nb}) and tensile stress area (A_s).

(2) Mechanical properties:

- Brace, column and gusset plate: yield stress (f_y) and ultimate stress (f_u).
- Bolts: ultimate stress ($f_{y,b}$) and yield stress ($f_{u,b}$).

4. Finite element model of the joint

In order to achieve the behaviour of the connection with a satisfactory level of accuracy, a large number of assumptions from a structural point of view and their application in the software need to be implemented. The numerical model used in this study was developed using ABAQUS/explicit dynamic solver (Dassault Systèmes, 2014). This solver was chosen over ABAQUS/Standard (Hibbit *et al.*, 2001) due to the usual convergence issues of the implicit solver. For an explicit dynamic solver, to be efficiently used for quasi-static analysis, the calculation speed needs to be increased artificially. This was achieved by mass scaling (Dassault Systèmes, 2014). Although in the short term, it implies that additional parameters should be tuned, in the long run, it creates a more stable model for manipulation.

4.1 Material models

The material model used for all joint elements (column, brace, gusset plate and bolts) is an elastic–perfectly plastic material model. For the end regions of members, elastic material model was applied. The material used for column, brace and gusset plate is S355 steel grade with 355 MPa of yield stress and elastic modulus of 210 GPa. The bolts are 10.9 high-strength steel with a yield strength of 900 MPa, Young's modulus of 210 GPa and Poisson's ratio of 0.3.

4.2 Element types

In ABAQUS software, a wide range of elements is provided to be used for different geometry and analysis types. The solid elements in ABAQUS software can be used for linear analysis as well as for complex non-linear analyses, taking into account contact, plasticity, allowable penetration and large deformations.

In this model, different element types are used. It is assumed that the end regions of members (pylon and brace) can be used for dimensional reduction. Therefore, the whole model combines the reduced dimensional element type (continuum shell) with higher dimensional elements (solid elements).

It is very important to integrate into the analysis of appropriate coupling between different element types. Therefore, a simple FE model is created to compare three cases with different element types and to address the coupling technique. Models with solid element type, continuum shell element type and combination of solid and continuum shell were studied (ASCE, 2000). The shell-to-solid combination was implemented using a surface-based technique for coupling shell elements to solid elements available in ABAQUS software. The geometry and boundary conditions of the plate are given in Figure 10. The plate is 600 mm long, 100 mm wide and 10 mm thick.

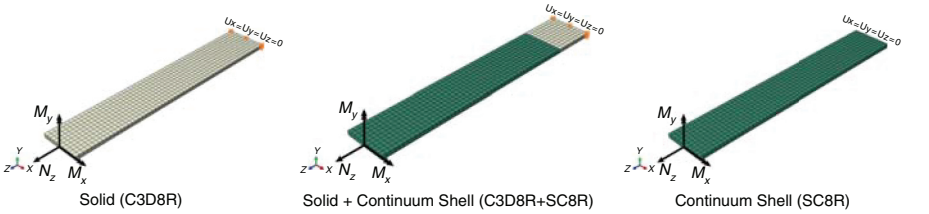

Figure 10.
Models with different element types

Material properties used in this case are ideal plastic steel S355 with a yield point at f_y=355 MPa, modulus of elasticity of E=210,000 MPa and Poison's ratio of ν=0.3. Elastic–perfectly plastic stress–strain curve is applied. Rigid-body constraint is defined at the end of the plate with the reference point (RP) in the centre of the cross-section. The load is applied in the RP in three steps, with each following the initial step. The loads applied are N_z=−300 kN, M_y=5 kNm (major bending) and M_x=0.5 kNm (minor bending).

Displacement at the end of the beam is compared between different element types for all three load cases and compared with analytical calculation as well (Table IV).

A good correlation between results is obtained. Therefore, for the further analysis, a combination of solid elements in the connection part tied with continuum elements at the end of the members is used.

Regarding the stress distribution, for minor bending loading and in the contact region between two element types, different stresses on the surface are observed (Figure 11). This difference is due to the stresses that are computed at the element surface in the case of continuum shell elements and the stresses that are computed at the integration point, which is in the middle of the element for the C3D8R, in the case of the solid elements.

4.3 Interactions

FE models are considered and three types of interactions are implemented, which are described as follows:

(1) Rigid-body constraint: it simulates the planar behaviour of a cross-section and integrates the global mechanic response (both in terms of kinematic and internal

	Analytical (mm)	Solid (mm)	Solid + CS (mm)	CS (mm)
Axial	0.857	0.853 (0.5%)	0.850 (0.8%)	0.848 (1.0%)
Major bending	5.143	5.181 (0.8%)	5.144 (0.0%)	5.104 (0.8%)
Minor bending	51.43	54.18 (5.3%)	51.83 (0.8%)	50.88 (1.1%)

Table IV. Displacements at the end of the plate

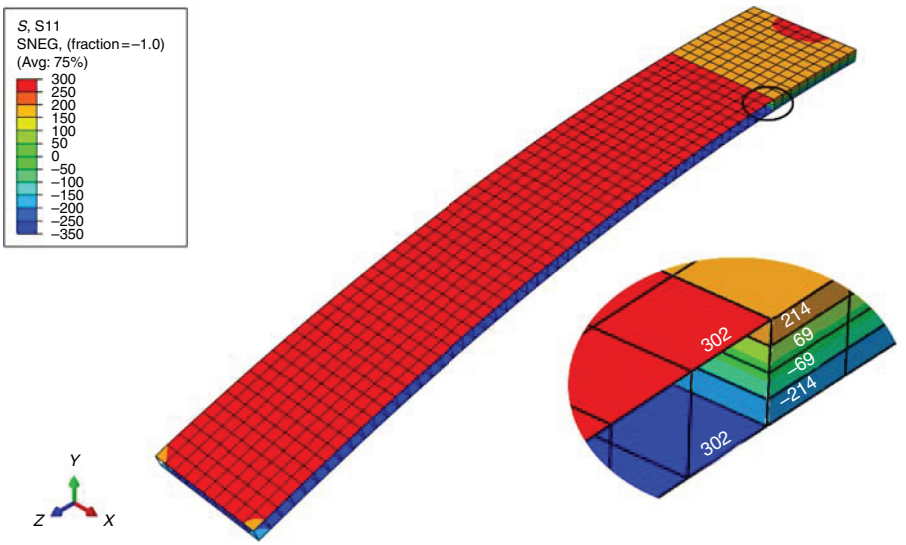

Figure 11. Stress distribution at the contact in the solid + CS element type models

forces) of the whole section. Due to this type of constraint, it is possible to define RPs and apply the boundary condition of the entire section in these points (Figure 12).

(2) Tie constraint: it connects two surfaces in a way that there is no relative displacement between them. It is used to simulate the weld connection between the gusset plate and the welded pylon. It was also used in bolted connections along with the elements outside of the connection. Moreover, this type of constraint was used to represent the contact between solid and continuum shell elements.

(3) Contact interaction: it represents the interaction between surfaces, which is characterized by friction sliding without penetration. The "Coulomb friction" is used with the aim to represent tangential behaviour. In this analysis, the used friction coefficient takes the value of 0.4. To represent the normal behaviour, the "Hard contact" is used. This interaction must be applied to the surfaces of the bolt shank and hole; the surface of the bolt head and nut and the corresponding surfaces of the pylon, brace or gusset plate; and the surfaces in contact between gusset plate and pylon, brace or plate.

4.4 Boundary conditions, load application and analysis type

The analysis type is ABAQUS/explicit dynamic. It is carried out in two steps: clamping, in which bolt preload is applied, and monotonic load, with the final displacement (δ) taking the value of 200 mm in the vertical direction, as shown in Figure 12. The load is applied using the

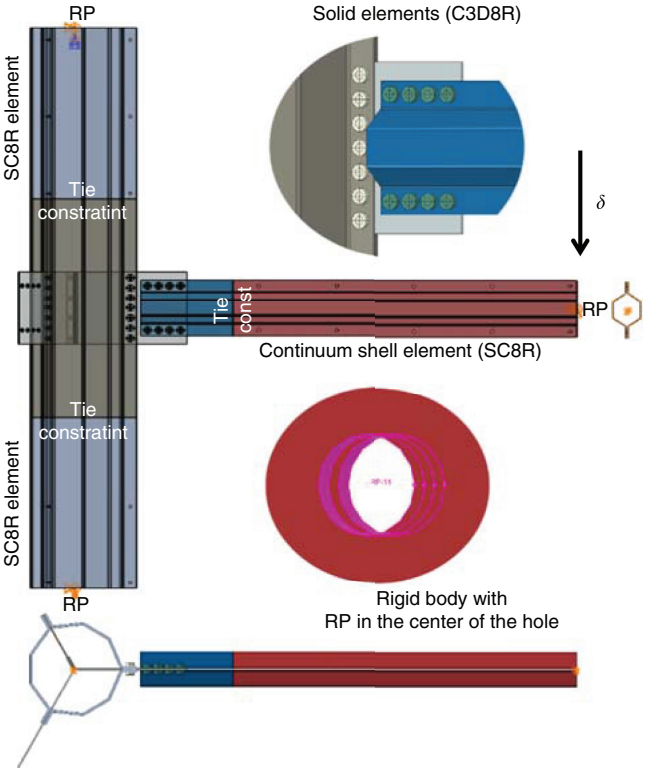

Figure 12.
Interactions and boundary conditions

"Explicit Dynamic" method including the non-linear effects of large displacements. Smooth amplitude functions are used for all loading steps, which change in boundary conditions, to withdraw impact behaviour and excitation of the model due to inertia forces.

4.4.1 Bolt preload model. Solid FEs, C3D8R, were used to model a simplified geometry of the bolts (Figure 13). The following simplifications are made:

(1) the bolt shank is modelled as a cylinder with a diameter equal to the nominal diameter of the bolt (d_b);

(2) in order to reduce the number of contact regions, washers are excluded; and

(3) bolts along the elements are not modelled.

For the tightening force of the bolts, a preload was applied as a thermal contraction of the bolt part that represents the shank. In the material properties of the bolt, shank expansion is defined as an orthotropic expansion, with $\alpha_{11}=\alpha_{22}=0$ and $\alpha_{33}=\alpha$. The negative temperature is applied as a predefined field of the type temperature in the clamping step. The variation of the section is defined as constant through the region. The applied temperature is determined using the following relations:

$$\Delta T = \alpha \frac{\Delta l}{l_{shank}}, \tag{1}$$

$$\Delta l = \delta_{joint} \cdot F_{s.Rd}, \tag{2}$$

where α is the coefficient of thermal expansion, $F_{s.Rd}$ is the bolt preload force and δ_{joint} is elastic resistance of bolted connection (Pavlović *et al.*, 2015).

Elastic resistance of bolted connection is calculated according to the VDI Guideline (VDI – Association of German Engineers (2003)). It represents the sum of elastic resistance of the preloaded bolt δ_{bolt} and the elastic resistance of the clamping package (steel plates and bolt head and nut) δ_{cp}:

$$\delta_{joint} = \delta_{bolt} + \delta_{cp}. \tag{3}$$

According to VDI Guideline, the elastic resistance of preloaded bolt takes into elastic deformation within clamping length as well as the elastic deformations outside of the clamping length region that have an influence on the deformation behaviour of the bolt in the joint. The bolt model considered consists of three individual elements: the head, the shank and the nut. As in a bolt, the cylindrical elements are arranged in a row, the total resistance of a

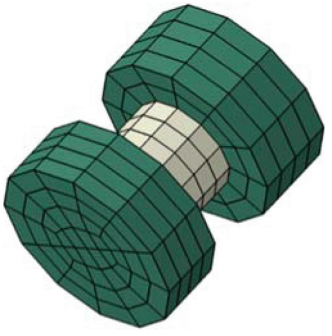

Figure 13.
Solid bolt model

bolt is determined by adding the resistance of individual cylindrical elements within the clamp length and further deformation regions:

$$\delta_{bolt} = \delta_{head} + \delta_{shank} + \delta_{nut}, \tag{4}$$

where:

$$\delta_{head} = \frac{l_{head}}{E_{bolt} \cdot A_{nom}} \quad l_{head} = 0.5d \quad A_{nom} = \frac{\pi}{4} d^2, \tag{5}$$

$$\delta_{shank} = \frac{l_{cp}}{E_{bolt} \cdot A_{nom}} \quad l_{cp} = l_{shank}, \tag{6}$$

$$\delta_{nut} = \frac{l_{nut}}{E_{bolt} \cdot A_{nom}} \quad l_{head} = 0.5d. \tag{7}$$

For concentrically clamped bolted joint, the elastic resistance of clamped parts is calculated according to the following expression that is valid in the case of $D_A \geqslant D_{A,Gr}$:

$$\delta_{cp} = \frac{2 \ln[((d_w + d_0) \cdot (d_w + l_{cp} \cdot \tan \varphi - d_0))/((d_w - d_0) \cdot (d_w + l_{cp} \cdot \tan \varphi + d_0))]}{E_{cp} \cdot \pi \cdot d_h \cdot \tan \varphi}, \tag{8}$$

where d_w is the outside diameter of washer $= d_{nb} = d_{hb}$, l_{cp} is the clamping package length, ϕ is the deformation angle taken as $\phi = 35°$ and E_{cp} is clamping package Young's modulus (plates).

The preload force in the bolts obtained after applying the calculated temperature is lower than $F_{s.Rd}$. Therefore, the temperature must be calibrated (Liu *et al.*, 2019). Table V presents the temperatures that were calculated and calibrated, and the corresponding preloading forces for B90 case. The bolt diameter is M20 for which $F_{s.Rd} = 172$ kN, according to EN 1993-1-8. The preloading forces obtained in the first iteration, for calculated temperature, are 10 and 19 per cent lower than $F_{s.Rd}$ for brace and column bolts, respectively (Figure 14).

4.4.2 Load application. In the first step, a bolt load is applied through a thermal contraction with a duration of the 50 s. In the second step, the actuator displacement (δ) of 200 mm (vertical direction as shown in Figure 12) was applied over a period of 500 s. The displacement control loading is applied in a smooth manner, as shown in Figure 15, in order to diminish the inertia effects in quasi-static analysis using an explicit dynamic solver.

The maximum stable integration time increment for ABAQUS/explicit dynamic solver is obtained from the size of the smallest FE in the model divided by a wave propagation speed. Hence, it can result in an inapplicable long computational time. The calculation speed can be increased using two methods: time scaling or mass scaling (Dassault Systèmes, 2014). Either of these methods can lead to an increase in inertia forces in the model, which might lead to meaningless results. Therefore, a compromise between the quality of results and acceptable computational time must be found. For these analyses, mass scaling with a time increment of 0.005 was applied. The FE masses are automatically increased, so their stable time increment matches the desired time increment (Dassault Systèmes, 2014). For these models, with a large

Table V. Applied temperature and obtained preloading force

Clamping length (mm)	Calculated T (°C)	Preloading force (kN)	Calibrated temperature (°C)	Preloading force (kN)
16	−697	155 (10%)	−772	172
30	−494	139 (19%)	−608	172

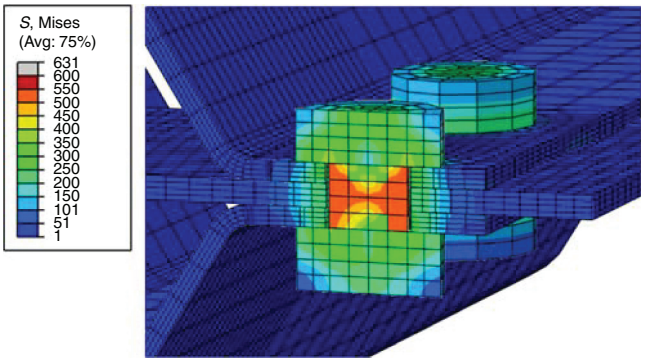

Figure 14.
Bolt model subjected to thermal loading

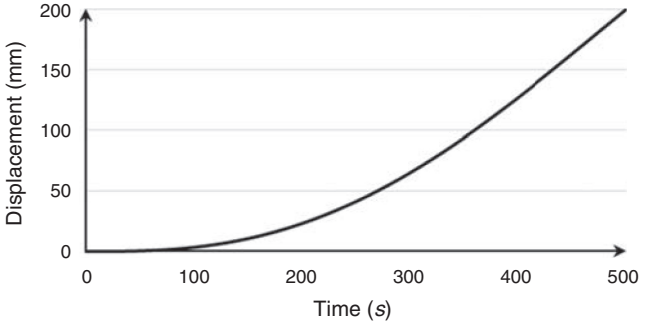

Figure 15.
Amplitude of applied displacement

range of element sizes, mass scaling is set to be variable (recomputed in every integration step) and non-uniform (different for each FE).

Mass scaling factor applied was obtained by matching input and output forces in a model for displacement controlled failure loading. Several analyses decreasing mass scaling factor were carried out, as shown in Figure 16. Linear matching curve without fluctuations for the smallest time increment ensures that no inertia effects govern the results (Figure 16).

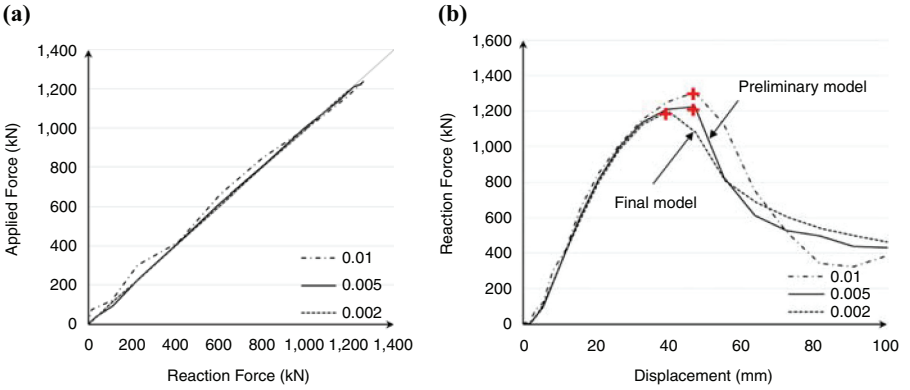

Figure 16.
Mass scaling factor

Notes: (a) Applied force vs reaction force; (b) reaction force vs displacement

The use of explicit solver in this study is for a quasi-static model. Therefore, it is critical to keep the kinetic energy to a minimum (KE/IE ratio less than 5–10 per cent). The energy ratio is presented in Figure 17. The kinematic energy is below 5 per cent of inertia energy through simulation; therefore, analysis can be considered quasi-static.

5. Resistance of connections

The moment–rotation curve is used to represent the connection behaviour. In this research, the moment–rotation curve was used with the aim of adjusting the FE model based on a comparison between the obtained ultimate resistance and the results obtained using EC3 (European Committee for Standardisation, 2010). This curve is presented by the relationship between the bending moment ratio, M_j/M_y, and the corresponding rotation ratio, θ_j/θ_y. Bending moment, M_j, corresponds to the applied moment to a joint, whereas rotation, θ_j, is the rotation between the connected members. Bending moment, M_y, and rotation, θ_y, are, respectively, the plastic resistance of brace and the yield rotation of the brace determined according to FEMA 356 (ASCE, 2000):

$$\theta_y = \frac{W_{pl} \cdot f_y \cdot L_b}{6 \cdot E \cdot I_b}. \tag{9}$$

The bending moment of the connection corresponds to the applied load ($R3_{RP3}$) multiplied by the distance between the centre of the pylon and the end of the brace (L_{load}), as stated in the following relation:

$$M = R3_{RP3} \cdot L_{load}. \tag{10}$$

In Figure 18, the displacement values in the RPs (P_1, P_2, B_1, B_2) are used to evaluate the rotational deformation of the joint:

$$\theta = \frac{u_{1(B1)} - u_{1(B2)}}{h_{br}} - \frac{u_{1(P1)} - u_{1(P2)}}{h_{gp}}, \tag{11}$$

where u_1 is the horizontal displacement, h_{br} is the distance between points B_1 and B_2 and h_{gp} is the distance between points P_1 and P_2.

The results from FE models were compared with simplified design models based on EN 1993-1-8 rules. There are two main observations. First, the ultimate resistance from FE models is higher than from EC3, probably due to a more conservative approach of Eurocode. The second observation is that the failure modes suggested by von Mises plastic strain from finite element analysis (FEA) are correlated with EC3.

For B90, a gusset plate net-section failure was detected, as can be seen in Figure 19. Moreover, gusset plate bearing in the position of end pylon bolt was obtained both

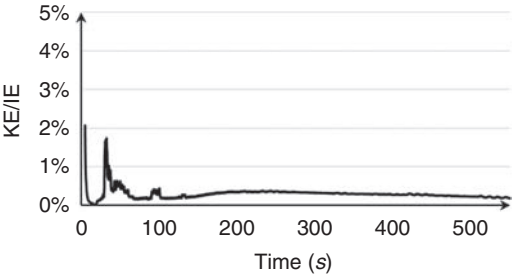

Figure 17.
Quality of quasi-static solution

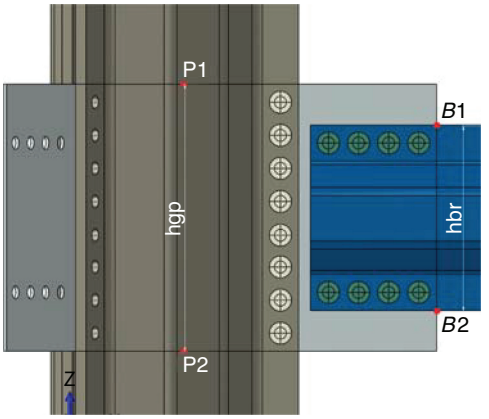

Figure 18.
Moment and rotation calculation parameters

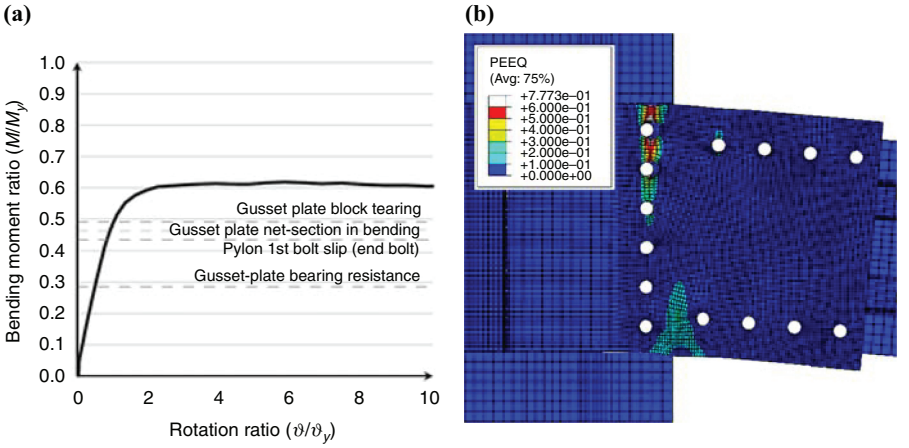

Figure 19.
B90 – gusset plate net-section failure

Notes: (a) Moment–rotation curve; (b) FEM failure mode

analytically and in FEA. Analytically, the lowest resistance was obtained for gusset plate bearing, and it is 4 per cent lower than for the gusset plate considering the net-section resistance. The ultimate resistance obtained analytically is 26 per cent lower than one obtained from FEA.

By its turn, B45 failure mode is gusset plate buckling (Figure 20). The same failure mode was obtained both analytically and in FEA. The ultimate resistance obtained analytically is 19 per cent lower than one from FEA.

In the W90 case, the observed failure was brace net-section failure combined with brace bearing resistance (Figure 21). The analytical result shows that brace net-section resistance is 8 per cent higher compared to brace bearing resistance. FEA ultimate resistance is equal to brace bearing resistance. Brace block tearing, whose resistance according to analytical calculation is 1 per cent higher than brace bearing resistance, was not observed in FEA.

Finally, in W45, brace block tearing was observed as failure mode both analytically and in FEA, with 38 per cent higher resistance obtained in FEA (Figure 22).

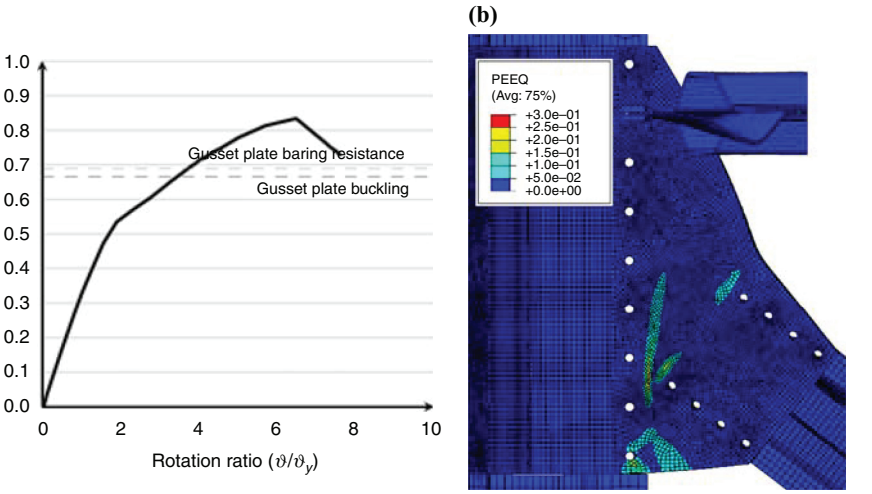

Figure 20.
B45 – gusset plate buckling

Notes: (a) Moment–rotation curve; (b) FEM failure mode

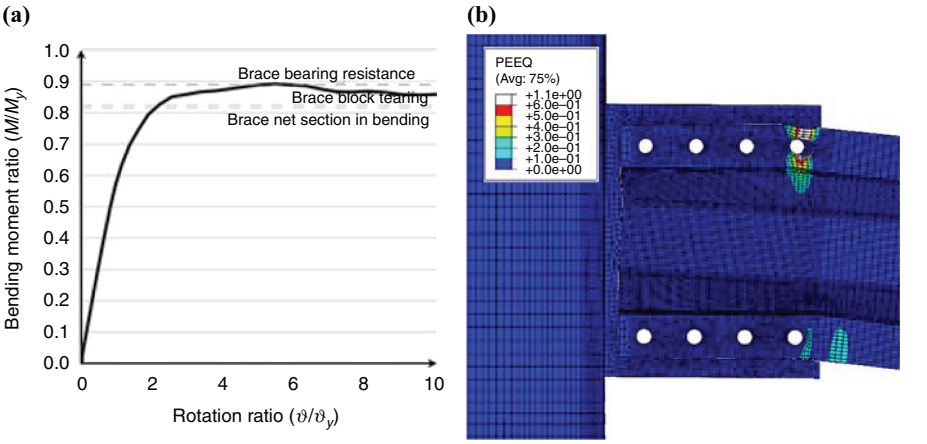

Figure 21.
W90 – brace net-section failure

Notes: (a) Moment–rotation curve; (b) FEM failure mode

6. Conclusion

The work presented in this paper deals with the design of a hybrid lattice–tubular wind tower structure. A large set of different geometries was considered in order to achieve the lightest structure, considering also the minimal number of connections and bolts per connection. Based on results, it is possible to conclude that the six "legs" solution with *K* braces under 45° angle and *H/S* ratio of 4/1 and 5/1 provides the most suitable balance between the weight of the supporting structure, the number of bolts in joints and reaction forces in the foundations. The six-legged tower with *H/S*=5/1 has 33 per cent fewer bolts and 10 per cent lower reaction forces compared to the lightest solution (four-legged tower with *H/S*=5/1) whose structure is 16 per cent lighter.

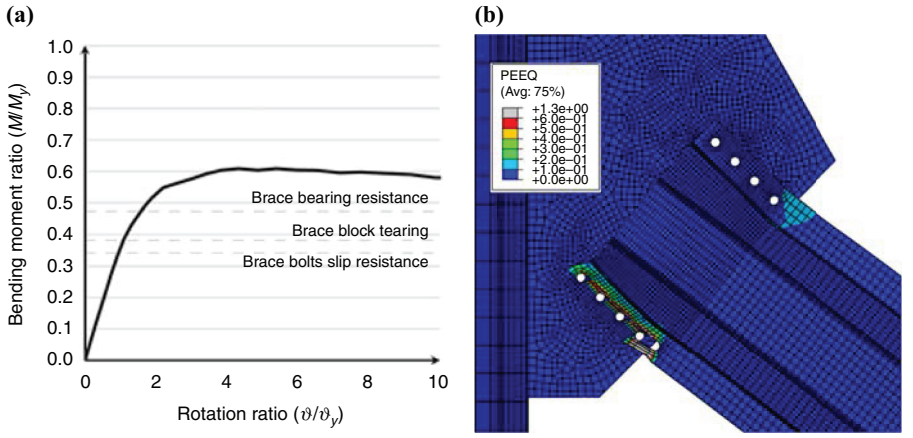

Notes: (a) Moment–rotation curve; (b) FEM failure mode

Figure 22.
W45 – brace block tearing

Furthermore, a typical joint in this type of tower was investigated numerically in more detail. The 3D FE models were created. The analyses were carried out using ABAQUS/explicit dynamic solver in order to overcome convergence problems and decrease computational time.

Moreover, different types of elements were used: solid elements and continuum shell elements. For the rectangular cantilever beam, composed of solid, solid + CS and CS elements, in axial, major and minor bending load case, the displacement at the end of the beam differs for up to 1.1 per cent compared to results obtained using elastic beam theory (except for solid elements model in minor bending where this difference is 5.3 per cent). Therefore, the solid + CS model was chosen for further study. For the tightening force of the bolts, the thermal contraction of the bolt shank was used. Analytical procedure was used to calculate applied temperate results in lower preload force than $F_{s.Rd}$. The difference for the studied case was up to 19 per cent, depending on clamping length. Therefore, the applied temperature must be calibrated in order to achieve $F_{s.Rd}$.

The FE results were compared with analytical calculation according to EC3-1-8. The comparison revealed that FE models are able to accurately predict the failure mode of the joint, while overestimating the design moment resistance for 26 per cent in case of gusset plate net-section failure, 19 per cent in case of gusset plate buckling, 8 per cent in case of brace net-section failure and 38 per cent in case of brace block tearing failure. These differences can be attributed to a more conservative approach of Eurocode.

The experimental testing on joints will be carried out in the near future to validate the results obtained from FE models. The parametric study will follow, and hand calculation model that takes into account joint tolerances for assembly will be developed.

References

ASCE (2000), "Prestandard and Commentary for the Seismic Rehabilitation of Buildings", FEMA-356, American Society of Civil Engineers, Washington, DC.

Alvarez-Anton, L., Koob, M., Diaz, J. and Minnert, J. (2016), "Optimization of a hybrid tower for onshore wind turbines by building information modeling and prefabrication techniques", *Visualization in Engineering*, Vol. 4 No. 1, pp. 1-9.

Américo, P., Magalhães Júnior, P.A.A., Rios, I.G., Ferreira, T.S., De Andrade Júnior, A.C., De Carvalho Filho, O.A. and Soares, P.H.D. (2014), "Design of lattice wind turbine towers with structural

optimization", *International Journal of Engineering Research and Applications*, Vol. 4 No. 8, pp. 38-51.

Bulson, P.S. (1969), "The strength of thin walled tubes formed from flat elements", *International Journal of Mechanical Sciences*, Vol. 11 No. 8, pp. 613-620.

Dassault Systèmes (2014), "Abaqus Analysis User's Manual version 6.14".

Duthoit, M. and Falzarano, J. (2018), "Assessment of the potential for the design of marine renewable energy systems", *Ocean Systems Engineering*, Vol. 8 No. 2, pp. 119-166.

European Committee for Standardisation (2010), "EN 1993-1-8:2005 Eurocode 3: Design of Steel Structures – Part 1-8 : Design of Joints", Vol. 3, Brussels.

EWEA (2015), "The European offshore wind industry key 2015 trends and statistics", Brussels.

EWEA (2017), "Wind energy in Europe: scenarios for 2030", European Wind Energy Association, Brussels.

Farhan, M., Mohammadi, M.R.S., Correia, J.A. and Rebelo, C. (2018), "Transition piece design for an onshore hybrid wind turbine with multiaxial fatigue life estimation", *Wind Engineering*, Vol. 42 No. 4, pp. 286-303.

Figueiredo, G. and Carlos, R. (2013), "Structural behaviour of hybrid lattice – tubular steel wind tower", Univesity of Coimbra, Coimbra.

Garzon, O. (2013), "Resistance of Polygonal Cross-Sections – Application on Steel Towers for Wind Turbines", Luleå University of Technology, Lulea.

Gencturk, B., Attar, A. and Tort, C. (2012), "Optimal design of lattice wind turbine towers", 15 WCEE, Lisbon.

Gencturk, B., Attar, A. and Tort, C. (2014), "Selection of an optimal lattice wind turbine tower for a seismic region based on the Cost of Energy", *KSCE Journal of Civil Engineering*, Vol. 19 No. 7, pp. 2179-2190.

General Electric – Renewable Energy (2014), "Space frame tower", General Electric, Amsterdam, p. 2.

Gong, W. (2011), "Lattice tower design of offshore wind turbine support structures", master's thesis, NTNU, Trondheim.

Hau, E. (2006), *Wind Turbines: Fundamentals, Technologies, Application, Economics*, Springer, Berlin.

Heistermann, C. (2011), "Behaviour of pretensioned bolts in friction connections", Luleå University of Technology, Lulea.

Hibbit, D.K.B., Karlsson, B.I. and Sorenson, P. (2001), "User's Manual I-III, version 6.3", *ABAQUS/ Standard*, Hibbit, Karlsoon and Sorenson.

Jaspart, J.P. and Weynand, K. (2016), "Design of joints in steel and composite structures", European Convention for Constructional Steelwork (ECCS), Brussels.

Jovašević, S., Rebelo, C., Pavlović, M. and Veljković, M. (2017), "Numerical investigation of preloaded gusset plate connections between polygonal built-up members", *Proceedings of Eurosteel*, pp. 292-297.

Jovašević, S., Shah Mohammadi, M.R., Rebelo, C., Pavlović, M. and Veljkovic, M. (2017), "New Lattice-Tubular Tower for Onshore WEC – Part 1: structural optimization", *Procedia Engineering*, Vol. 199, pp. 3236-3241.

Letcher, T.M. (2017), "Why wind energy?", in Letcher, T.M. (Ed.), *Wind Energy Engineering*, Academic Press, London, pp. 3-14.

Liu, Z., Correia, J., Carvalho, H., Mourão, A., de Jesus, A., Calçada, R. and Berto, F. (2019), "Global-local fatigue assessment of an ancient riveted metallic bridge based on submodelling of the critical detail", *Fatigue & Fracture of Engineering Materials & Structures*, Vol. 42 No. 2, pp. 546-560.

Mohammadi, M.R.S., Richter, C., Pak, D., Rebelo, C. and Feldmann, M. (2018), "Steel Hybrid Onshore Wind Towers Installed with Minimal Effort: development of lifting process", *Wind Engineering*, Vol. 42 No. 4, pp. 335-352.

Muskulus, M. (2012), "The full-height lattice tower concept", *Energy Procedia*, Vol. 24, January, pp. 371-377.

Muskulus, M. and Schafhirt, S. (2014), "Design optimization of wind turbine support structures – a review", *Journal of Ocean and Wind Energy*, Vol. 1 No. 1, pp. 12-22.

Nunez-Casado, C., Lopez-Garcia, O., de las Heras, E.G., Cuerva-Tejero, A. and Gallego-Castillo, C. (2017), "Assembly strategies of wind turbine towers for minimum fatigue damage", *Wind and Structures*, Vol. 25 No. 6, pp. 569-588.

Ozturk, F., Rebelo, C. and Correia, J.A. (2016), "Finite element modelling of tubular bolted connection of a lattice wind tower for fatigue assessment", University of Coimbra, Coimbra.

Pavlović, M., Heistermann, C., Veljković, M., Pak, D., Feldmann, M., Rebelo, C. and Simões da Silva, L. (2015), "Connections in towers for wind converters, Part II: the friction connection behaviour", *Journal of Constructional Steel Research*, Vol. 115, December, pp. 458-466.

Rebelo, C., Correia, J., Baniotopoulos, C. and Jesus, A. De (2018), "Wind energy technology (WINERCOST)", *Wind Engineering*, Vol. 42 No. 4, p. 267.

Ruukki (2011), "Ruukki wind towers: reaching the heights with Ruukki", Helsinki.

Seidel, M., Voormeeren, S. and van der Steen, J.-B. (2016), "State-of-the-art design processes for offshore wind turbine support structures", *Stahlbau*, Vol. 85 No. 9, pp. 583-590.

SHOWTIME (2014), "EC-RFSR-CT-2015-00021-SHOWTIME – steel hybrid onshore wind towers installed with minimal effort", Project proposal report, European Union.

Suzlon Energy Limited (2016), *2.1 MW PLATFORM S97-S111*, Suzlon Group, pp. 1-12.

VDI – Association of German Engineers (2003), "VDI Guideline – Part I, Systematic calculation of high duty bolted joints – Joints with one cylindrical bolt".

Vestas Wind Systems A/S (2016), "Large diameter steel flanges (LDST)", VESTAS, Aarhus, pp. 1-2.

Wang, L., Kolios, A., Luengo, M.M. and Liu, X. (2016), "Structural optimisation of wind turbine towers based on finite element analysis and genetic algorithm", *Wind Energy Science Discussion*, Vol. 44, December, pp. 1-26.

Webber, A., Orr, J.J., Shepherd, P. and Crothers, K. (2015), "The effective lenght of columns in multi-storey frames", *Engineering Structures Journal*, Vol. 102, pp. 132-143.

Corresponding author
José Correia can be contacted at: jacorreia@fe.up.pt